VISCOUS PLASMA FLOW

IN A MULTIPLE-MIRROR CONFIGURATION

by

R. V. Bravenec, A. J. Lichtenberg, M. A. Lieberman and H. L. Berk

Memorandum No. UCB/ERL M80/56

8 January 1980

ELECTRONICS RESEARCH LABORATORY

College of Engineering
University of California, Berkeley
94720

VISCOUS PLASMA FLOW

IN A MULTIPLE-MIRROR CONFIGURATION

R. V. Bravenec, A. J. Lichtenberg, M. A. Lieberman

Department of Electrical Engineering and Computer Sciences
and the Electronics Research Laboratory
University of California, Berkeley, California 94720

H. L. Berk

Department of Physics
University of Texas, Austin, Texas 78712

ABSTRACT

The steady-state, axial plasma confinement by a multiple-mirror device is studied in the "viscous fluid regime," $\lambda/\ell_m \ll 1$ (but not negligible), where λ is the ion-ion mean-free-path and ℓ_m is the scale length of magnetic field variations. One-dimensional axial flow of an isothermal, low-β plasma ($\beta \equiv$ plasma pressure/magnetic field pressure) is considered. An approximate analytical solution is obtained by averaging over the rapid variations caused by the individual mirrors. This solution is compared to a numerical solution without averaging. There is found a smooth transition with increasing values of λ/ℓ_m from sonic flow in which the average density is uniform along the system to a diffusive flow. Studies are made of the variation in density profiles and confinement times versus λ/ℓ_m, mirror ratio, relative mirror width, and number of mirror cells. Using the scaling of the approximate analytical solution with the above parameters, an empirical equation is obtained for the confinement time which better fits the numerical results and exhibits the individual contributions to the confinement time of sonic

flow and diffusive flow. The viscous fluid regime is found to have the same characteristics as the ideal multiple-mirror regime for $\lambda/\ell_m \to 1$.

I. INTRODUCTION

A multiple-mirror device in its simplest form consists of a solenoidal magnetic field and a series of magnetic mirrors spaced by a "cell length" ℓ_c. The axial magnetic field for such a device is sketched in Fig. 1. Here ℓ_m is the scale length of magnetic field variations and $R_m \equiv B_{max}/B_{min}$ is the mirror ratio. In the "ideal multiple-mirror regime" in which $\ell_m \ll \lambda \ll R_m \ell_c$, where λ is the ion-ion mean-free-path, the axial loss process is diffusive and the confinement time scales quadratically with the number of cells (the system length L increasing with the number of cells).[1,2] In their analysis Makhijani et al.[1] used random-walk arguments while Mirnov and Ryutov[2] employed a kinetic description. Miller[3] applied a viscous fluid analysis to the ideal multiple-mirror regime by limiting the classical viscosity for large λ. In contrast to the ideal multiple-mirror regime, these devices must sometimes confine a highly collisional plasma, as during the initial fill of a laboratory experiment or startup of a conceptual reactor. In the ideal magnetohydrodynamic (MHD) regime in which $\lambda/\ell_m \to 0$, treated by Makhijani et al., the axial loss process is sonic flow and the confinement time scales linearly with the number of cells. Mirnov and Ryutov further considered the "viscous fluid regime," $\lambda/\ell_m \ll 1$ (but not negligible), and found a diffusive loss process. However, they restricted attention to sufficiently large values of λ/ℓ_m such that MHD flow effects were unimportant.

This paper unites the analysis of the MHD regime with that of the viscous fluid regime in order to better understand the transition from sonic flow to multiple-mirror diffusion with increasing values of λ. Exact numerical solutions of the viscous fluid equations are obtained and

compared to approximate analytical solutions, over a parameter range encompassing both dominantly flow and dominantly diffusive behavior. We assume the flow is steady, resulting from an arbitrary plasma source in the central cell and sinks at the ends. Radial motion is neglected by making a "long, thin approximation" with the axial magnetic field large enough to suppress any radial diffusion. Furthermore the plasma is assumed isothermal and of low β ($\beta \equiv$ plasma pressure/magnetic field pressure). Isothermy originates from a large electron thermal conductivity which maintains the electron temperature uniform along the device. To lowest order the ion temperature equilibrates on the time scale $\tau_{ie} \sim (m_i/m_e)^{\frac{1}{2}}\tau_{ii}$, where τ_{ie} and τ_{ii} are the ion-electron and ion-ion scattering times,[4] and m_e and m_i are the electron and ion masses. For a low-β plasma the magnetic field is a known function of the axial coordinate. Through conservation of magnetic flux the plasma cross section is also known.

Section II presents the fluid equations and the derivation of a second-order ordinary differential equation for the density. This equation is cast in dimensionless form to select out the important parameters of the problem and is referred to as the "flow equation." Section III presents an approximate analytical solution for the density profile by averaging the flow equation over the rapid variations caused by the individual mirrors. A confinement time is calculated and the nature of the particle flux is examined as a function of λ . Section IV presents direct numerical solutions of the flow equation and compares these to the analytical solutions. A study is made of the scaling of the confinement time with λ , R_m , ℓ_m/ℓ_c and the total number of cells N . Finally in Sec. V these results are summarized and related to the ideal multiple-mirror regime.

II. FORMULATION OF THE PROBLEM

A. The fluid equations

The following are adapted from Dawson and Uman,[5] applying the assumptions discussed in the introduction.

Force equation for the electrons:

$$0 = -\frac{d}{dz}(nkT) - enE \ . \tag{1a}$$

Force equation for the ions:

$$m_i nv\frac{dv}{dz} = -\frac{d}{dz}(nkT_i^{\parallel}) + enE + \frac{n_o^i}{A}\frac{d}{dz}(A\frac{dv}{dz}) + nk(T_i^{\perp} - T_i^{\parallel})\frac{1}{A}\frac{dA}{dz} \ . \tag{1b}$$

Continuity equation:

$$\frac{d}{dz}(nAv) = 0 \ . \tag{1c}$$

Perpendicular ion temperature equation:

$$0 = -\frac{(T_i^{\perp} - T_i^{\parallel})}{\tau_{ii}} + \frac{2n_o^i}{3nk}\left(\frac{dv}{dz}\right)^2 - \frac{T_i^{\perp}v}{A}\frac{dA}{dz}$$

$$+ \frac{1}{\tau_{ei}}\frac{m_e}{m_i}[T - (\frac{2}{3}T_i^{\perp} + \frac{1}{3}T_i^{\parallel})] \ . \tag{1d}$$

Parallel ion temperature equation:

$$0 = \frac{2(T_i^{\perp} - T_i^{\parallel})}{\tau_{ii}} + \frac{2n_o^i}{3nk}\left(\frac{dv}{dz}\right)^2 - 2T_i^{\parallel}\frac{dv}{dz} + \frac{1}{\tau_{ei}}\frac{m_e}{m_i}[T - (\frac{2}{3}T_i^{\perp} + \frac{1}{3}T_i^{\parallel})] \ . \tag{1e}$$

Magnetic flux conservation:

$$A = A_o \frac{B_o}{B} \quad . \tag{1f}$$

Here z is the axial coordinate, n is the ion (and electron) density, A is the plasma cross section, v is the z-component of the flow velocity (same for ions and electrons), T is the electron temperature (assumed uniform and isotropic), $T_i^{\parallel}$ and $T_i^{\perp}$ are the ion temperatures respectively parallel and perpendicular to the magnetic field, E is the axial electric field, B is the axial magnetic field, τ_{ei} and τ_{ii} are respectively the electron-ion and ion-ion scattering times, m_e and m_i are respectively the electron and ion masses, e is the electron charge, k is Boltzmann's constant, and $\eta_o^i = \alpha n \tau_{ii} k T_i^{\parallel}$ with $\alpha \simeq 1$ is the longitudinal ion viscosity. The reader is referred to Ref. 5 for a thorough discussion of these equations.

B. Derivation of the "flow equation"

The following steps are performed on Eq. (1b): First the difference of Eqs. (1d) and (1e) is solved for $T_i^{\perp} - T_i^{\parallel}$ and substituted into the last term. Hereafter we set $T_i^{\perp} = T_i^{\parallel} = T$. Equation (1a) is then used to eliminate the electric field. The resulting equation is rewritten in terms of the following dimensionless quantities:

$$\eta \equiv \frac{n}{n_o} \quad , \quad M \equiv \frac{v}{v_s} \quad , \quad \zeta \equiv \frac{z}{\ell_c} \quad , \quad a \equiv \frac{A}{A_o} \quad . \tag{2}$$

Here $n_o \equiv n(0)$, etc., and $v_s \equiv (2kT/m_i)^{\frac{1}{2}}$ is the sound speed. The normalized form of the continuity equation (1c),

$$\eta a M = M_o \,, \tag{3}$$

is used to eliminate M. Dividing the result by η, we obtain

$$\frac{M_o^2}{2}\frac{d}{d\zeta}\left(\frac{1}{\eta^2 a^2}\right) + \frac{1}{\eta}\frac{d\eta}{d\zeta} = \frac{\lambda_o}{\ell_c}\frac{M_o}{2}\left\{\frac{\alpha}{\eta a}\frac{d}{d\zeta}\left[a\frac{d}{d\zeta}\left(\frac{1}{\eta a}\right)\right] + \frac{a}{3}\frac{da}{d\zeta}\frac{d}{d\zeta}\left(\frac{1}{\eta^2 a^3}\right)\right\} \tag{4}$$

hereafter referred to as the "flow equation." (Use has also been made of the definition $\lambda \equiv v_s/\tau_{ii}$ and the relation[4] $\tau_{ii} \propto T^2/n$.) The terms on the left represent the ion inertia and scalar pressure, respectively, while the term on the right is due to pressure anisotropy (viscosity). The latter is seen to vanish with λ_o/ℓ_c .

The solution of Eq. (4) requires specification of λ_o/ℓ_c , M_o , $a(\zeta)$ and the region over which a solution is desired. We consider a multiple-mirror device with a central cell of arbitrary length, where the plasma source is located. This cell, for example, could be a theta-pinch for which the multiple-mirror cells play the role of end-stoppers. We will not consider this cell here but restrict attention to the region between one of its bounding mirrors and an end mirror as in Fig. 1. This region we define as $0 \le \zeta \le N/2$, where N is the total number of multiple-mirror cells. With this definition, $L \equiv N\ell_c$ is the total length of the system minus the length of the central cell. The Mach number at the origin, M_o , is not a free parameter as is λ_o/ℓ_c and is determined in the following section.

III. ANALYTICAL SOLUTIONS

A. The averaged density profile

For λ/ℓ_m sufficiently large, so that viscosity is not negligible, we expect $\eta(\zeta)$ to vary little over a cell and its derivatives to be small. We then average Eq. (4) over each cell by integrating between two adjacent mirrors. (The choice of mirrors rather than midplanes is made because of their dominant role in determining the solution, as will be evident shortly.) On the right-hand side of Eq. (4) we assume that all derivatives of η are small compared to those of a and then remove η from beneath the averaging integral. After some algebra, Eq. (4) reduces to

$$\frac{M_o^2}{2}\frac{d}{d\zeta}\left(\frac{1}{\eta^2}\right)+\frac{1}{\eta}\frac{d\eta}{d\zeta} = -\frac{\lambda_o}{\ell_m}\frac{1+\alpha}{2}\frac{fM_o}{\eta^2} \qquad (5)$$

where

$$f \equiv \frac{\ell_m}{\ell_c}\int_0^1 \frac{d\zeta}{a^3}\left(\frac{da}{d\zeta}\right)^2 .$$

The details of the magnetic field are seen to appear only through the constant f. (The motive for including the factor ℓ_m/ℓ_c in the definition of f will become transparent later on.)

Solving Eq. (5) implicitly for $\eta(\zeta)$ we obtain

$$\eta^2 - M_o^2 \ell n\, \eta^2 = 1 - 2\frac{\lambda_o}{\ell_m} fM_o\zeta . \qquad (6)$$

(Here and in the remainder of the report α is set to unity.) There are

two distinct solutions depending on whether $M_o < 1$ (subsonic flow) or $M_o > 1$ (supersonic flow). These are sketched in Fig. 2. The profiles turn over ($d\eta/d\zeta \to \pm\infty$) at $\zeta = \zeta_1$, where

$$\zeta_1 = \frac{\ell_m}{\lambda_o} \frac{1 - M_o^2 + M_o^2 \ell n\, M_o^2}{2fM_o} \tag{7}$$

which marks the location where $\eta = M_o$ and $M = 1$. In subsonic fluid flow through a nozzle in which the exit pressure is low, the flow is choked ($M = 1$) in the nozzle.[6] By analogy, we asume choking in the last mirror throat and set $\zeta_1 = N/2$, resulting in an equation implicitly determining $M_o(\lambda_o/\ell_m , f , N)$. In the limit $\lambda_o/\ell_m \ll (fN)^{-1}$, this equation yields

$$M_o = 1 - \left(\frac{\lambda_o}{\ell_m} \frac{fN}{2}\right)^{\frac{1}{2}} \approx 1 . \tag{8a}$$

In the opposite limit $\lambda_o/\ell_m \gg (fN)^{-1}$ we have

$$M_o = \frac{\ell_m}{\lambda_o} \frac{1}{fN} \ll 1 . \tag{8b}$$

B. Interpretation of the flow

We briefly return to Eq. (5) to examine the nature of the particle flux. Rewriting in terms of n , v , A and z and defining the particle flux $F \equiv n_o v_o A_o$, we obtain a quadratic equation for F . Solving,

$$F = -\frac{\beta}{2} \pm \left[\left(\frac{\beta}{2}\right)^2 + \delta^2\right]^{\frac{1}{2}},$$

where

$$\beta \equiv n_o v_s A_o \frac{\lambda_o}{\ell_m} f\eta \left|\frac{d\eta}{d\zeta}\right|^{-1},$$

$$\delta \equiv n v_s A_o .$$

For $\delta \gg \beta$,

$$F = \delta = n v_s A_o ,$$

a result indicative of sonic flow, in which the average density is uniform and $M = 1$ in each mirror throat.

For $\delta \ll \beta$,

$$F = \frac{\delta^2}{\beta} = -n_o v_s A_o \frac{\ell_m}{\lambda_o} \frac{\eta}{f} \frac{d\eta}{d\zeta} ,$$

a result characteristic of a diffusive flow. A diffusion coefficient may be defined via $F \equiv -D(dn/dz)\bar{A}$, where $\bar{A}$ is the area averaged over a cell. With this definition

$$D = \frac{\ell_m}{\ell_c} \frac{\eta}{R_m f g} \frac{\ell_c^2}{\tau_{ii_o}} , \qquad (9)$$

where

$$g \equiv \frac{1}{R_m}\int_0^1 d\zeta \; a .$$

For general multiple-mirror fields $g \to 1$ for $\ell_m/\ell_c \to 0$. This expression for D differs from that of Mirnov and Ryutov only in that their values are smaller by the numerical factor 0.71. This discrepancy can be attributed to the slightly different form of the viscosity term used in their analysis.

The condition $\delta \ll \beta$ can be shown to be equivalent to $M \ll 1$, which implies both that $M_o \ll 1$ and that we are far from the ends of the device (where $M \equiv 1$). Thus, the condition leading to Eq. (8b), namely $\lambda_o/\ell_m \gg (fN)^{-1}$, specifies diffusive flow near the origin, while the opposite limit specifies sonic flow.

C. Calculation of the confinement time

The confinement time of the system is defined here as

$$\tau_c \equiv \frac{1}{F}\int_0^{L/2} dz\, nA = \left(\frac{2}{NM_o}\int_0^{N/2} d\zeta\, \eta a\right)\frac{L}{2v_s} . \qquad (10a)$$

By this definition τ_c for a straight solenoid ($a = 1$) is $L/2v_s$. Thus the quantity in parentheses represents the enhancement of this time by the mirrors. If η does not vary significantly over a cell

$$\tau_c \approx \left(\frac{2g}{NM_o} R_m \int_0^{N/2} d\zeta\, \eta\right)\frac{L}{2v_s} . \qquad (10b)$$

Evaluating this expression using Eq. (6) for η we obtain

$$\tau_c = R_m g \frac{L}{2v_s}\left\{1 + \frac{\ell_m}{\lambda_o}\frac{1}{fNM_o^2}\left[\frac{2}{3} - M_o - 2M_o^2 + M_o^3\left(\frac{7}{3} - \ell n\, M_o^2\right)\right]\right\}. \qquad (11a)$$

In the limit $\lambda_o/\ell_m \ll (fN)^{-1}$ we may use Eq. (8a) for M_o yielding

$$\tau_c = R_m g \frac{L}{2v_s}\left[1 + \frac{2}{3}\left(\frac{\lambda_o}{\ell_m}\frac{fN}{2}\right)^{\frac{1}{2}}\right]. \qquad (11b)$$

Thus, to a first approximation, the confinement time of a solenoid in the MHD limit $\lambda_o/\ell_m = 0$ is enhanced by the factor $R_m g$ due to the mirrors. This expression is to be compared to the low-β result of Makhijani et al., derived using an adiabatic equation of state,[1]

$$\tau_c \simeq \frac{16\sqrt{2}}{9} R_m \frac{L}{2v_s} ,$$

where v_s is evaluated in a midplane. This expression was derived in the limit $\ell_m/\ell_c \to 0$ ("point" mirrors), and represents an upper limit to the MHD confinement time. The numerical factor represents the enhancement of our expression by the effects of adiabaticity (slower sound speed in the mirror throats) and density maxima in the midplanes. This latter condition does not appear in our derivation, as will be borne out in the following section.

In the opposite limit $\lambda_o/\ell_m \gg (fN)^{-1}$, hereafter referred to as the "diffusive-flow regime",

$$\tau_c = \frac{2}{3}\frac{\lambda_o}{\ell_m} R_m f g N \frac{L}{2v_s} . \qquad (11c)$$

Thus we see that τ_c scales as L^2 (since $N \equiv L/\ell_c$) and also as λ_o/ℓ_m. We now explicitly evaluate the quantities f and g for the physical model of a solenoid plus a series of single loops of radius ℓ_m. These are calculated numerically for various values of R_m and ℓ_m/ℓ_c and

presented in Tables I and II. It is evident that f asymptotes to a function only of R_m as $\ell_m/\ell_c \to 0$, as can be shown analytically. Furthermore, f scales as $\ell n\, R_m$ for very large values of R_m. As mentioned earlier g approaches unity as $\ell_m/\ell_c \to 0$, and is less than unity for finite values of ℓ_m/ℓ_c. Thus, for a given value of λ_o/ℓ_c, τ_c as defined by Eq. (11c) is increased for large values of R_m and small values of ℓ_m/ℓ_c.

IV. COMPARISON WITH NUMERICAL SOLUTIONS

The flow equation (4) is solved numerically using the package GEAR written by Hindmarsh.[7] The code requires both boundary conditions to be specified at the starting point of the integration, these being M_o and $d\eta/d\zeta(0)$. These were determined as follows: A series of trial runs was made in which it was found that $d\eta/d\zeta \simeq 0$ in all midplanes regardless of the boundary conditions and input parameters. Hence, the integrations are initialized in a midplane where the condition $d\eta/d\zeta(0) = 0$ is imposed. (For $\lambda_o/\ell_c \ll 1$ the solutions are relatively insensitive to this choice.) A value of M_o is chosen and the package integrates to the last mirror throat where the value of M is examined by a controlling program. The code then varies M_o and begins again, repeating this cycle until $M = 1 \pm 0.1$ in the last mirror throat. The program also directly evaluates the confinement time, Eq. (10a), not including the initial half-cell.

The density profiles of three runs all with $R_m = 4$, $\ell_m/\ell_c = 0.1$ and $N = 18$ are shown in Figs. 3(a), 3(b), and 3(c) for $\lambda_o/\ell_c = 0.001$, 0.01, and 0.05, respectively. Superimposed are the profiles predicted by

Eqs. (6) and (7) with $\zeta_1 = N/2$. In the short mean-free-path case $\lambda_o/\ell_c = 0.001$ we observe that the density is sharply depressed in the mirror throats (Bernoulli flow), while the average level is significantly higher. Because of this, Eq. (6) underestimates the average density since the analytical profile follows the density in the mirror throats. We also note that the assumption $d\eta/d\zeta \ll da/d\zeta$ is violated on either side of a mirror, causing the analytical result to overestimate $M_o = \eta(N/2)$ by about 8% . In the long mean-free-path case $\lambda_o/\ell_c = 0.05$, a completely different type of profile exists which we call a "stairstep" pattern. The density is seen to be relatively uniform over each cell, changing levels when crossing the mirrors. Although the profile appears smoother than the short mean-free-path case, $d\eta/d\zeta$ is quite substantial at the mirrors where $da/d\zeta = 0$. This violates the assumptions leading to Eq. (6), causing the analytic solution to overestimate the density near the end. (We should note that at the end $\lambda/\ell_m = (\lambda_o/\ell_c)(\ell_c/\ell_m)/\eta \simeq 5$, which is clearly outside the range of validity of the fluid theory. Thus, this profile should be considered an extreme example of the limiting case $\lambda_o/\ell_m \gg (fN)^{-1}$, and should not be taken quantitatively.) For intermediate values of λ_o/ℓ_c the previously mentioned effects tend to cancel, leading to better agreement between the analytical and numerical results.

Values of confinement time are computed numerically and compared with those predicted by Eq. (11a). To investigate the scaling of τ_c with the four parameters λ_o/ℓ_c , R_m , ℓ_m/ℓ_c , and N , the data is presented in three formats. In Figs. 4(a), 4(b), and 4(c) we plot the ratio τ_c/τ_o , where $\tau_o \equiv 18\ell_c/2v_s$ is the confinement time of

a solenoid of length $18\ell_c$, versus λ_o/ℓ_c for three values of ℓ_m/ℓ_c, R_m, and N, respectively. The values of the remaining two parameters are in each case chosen from the set $R_m = 4$, $\ell_m/\ell_c = 0.1$, and $N = 18$. In Fig. 4(a), curves of constant λ_o/ℓ_m are included to indicate the relative independence of τ_c/τ_o on ℓ_m/ℓ_c for fixed λ_o/ℓ_m. The most striking feature of Fig. 4 is that the analytical values scale too rapidly with λ_o/ℓ_c, consistently underestimating τ_c for small λ_o/ℓ_c and overestimating τ_c for large λ_o/ℓ_c. This behavior results from the errors discussed in the previous paragraph. An empirical equation for τ_c can be obtained, using scalings of Eqs. (11b) and (11c), which better agrees with the numerical results, namely

$$\tau_c \simeq \left(1.6 + 0.45\,\frac{\lambda_o}{\ell_m}\,fN\right) R_m g\,\frac{L}{2v_s} \quad . \tag{12}$$

The first term represents the MHD limit in which the density maxima in the midplanes are included simply through the numerical factor 1.6. Although this factor actually varies slightly with R_m, ℓ_m/ℓ_c, and N, the above approximation agrees to within 5% of the numerical results of Fig. 4 extrapolated to $\lambda_o/\ell_c \equiv 0$. The second term of Eq. (12) represents the contribution of viscosity in which the numerical factor 0.45 serves to reduce the slopes of the curves τ_c versus λ_o/ℓ_c. This factor was chosen to make Eq. (12) best fit the numerical results with $R_m = 4$, $\ell_m/\ell_c = 0.1$, and $N = 18$. In total, Eq. (12) better models the numerical results of Fig. 4, the worst agreement being at $\lambda_o/\ell_c = 0.05$ for the case $R_m = 4$, $\ell_m/\ell_c = 0.1$, and $N = 8$ in Fig. 4(c) in which Eq. (12) predicts a value of τ_c/τ_o that is 19% too large.

V. SUMMARY AND DISCUSSION

In this work we have obtained a single expression, Eq. (12), for the steady-state multiple-mirror confinement time of an isothermal plasma in the viscous fluid regime $\lambda/\ell_m \ll 1$. In the limit $\lambda/\ell_m \equiv 0$ we recover the MHD regime in which the confinement time τ_c scales linearly with L (or N) and the average density is uniform along the device. Its dependence on ℓ_m/ℓ_c is weak since τ_c saturates with decreasing values of this parameter, in which case τ_c is seen to scale linearly with R_m. Comparing with the result of Makhijani et al. for adiabatic MHD flow in this same limit, we see that their expression is a factor of about 1.6 larger but also scales linearly with R_m. In the diffusive-flow regime $(fN)^{-1} \ll \lambda_o/\ell_m \ll 1$, we find a stairstep density variation and recover within a numerical factor the diffusion coefficient of Mirnov and Ryutov, which leads to a confinement time that scales quadratically with L (or N). It is found that for fixed values of λ_o/ℓ_c, the confinement time continually improves with decreasing values of ℓ_m/ℓ_c and that τ_c scales somewhat faster than R_m, going as $R_m \ell n\, R_m$ for $R_m \gg 1$.

Finally we relate our diffusive-flow regime to the ideal multiple-mirror regime $1 \ll \lambda/\ell_m \ll R_m \ell_c/\ell_m$ in which the confinement time in the limits $\ell_m/\ell_c \ll 1$ and $R_m \gg 1$ is roughly[1]

$$\tau_c^{max} \simeq \frac{\sqrt{\pi}}{4} R_m N \frac{L}{2v_s} . \qquad (13)$$

Both regimes are thus seen to scale quadratically with L (or N), although over the range of validity of the diffusive-flow regime $\tau_c \ll \tau_c^{max}$. In Fig. 5 we present a sketch of τ_c/τ_o in the limits

$R_m \gg 1$, $\ell_m/\ell_c \ll 1$, and $N \gg 1$, in which both Eqs. (12) and (13) are extrapolated into the region $\lambda_o/\ell_m \sim 1$. The dashed curve represents the form of the actual solution. Another similarity between the two regimes lies in the fact that the diffusive-flow regime can be described in terms of a diffusion coefficient. The ideal multiple-mirror regime is governed entirely by a classical diffusion process in which the particles random-walk from cell to cell, the diffusion coefficient being[1]

$$D_{min} = \frac{1}{\sqrt{\pi}} \frac{\lambda_o}{\ell_c} \frac{1}{R_m} \frac{\ell_c^2}{\tau_{ii_o}} \quad .$$

Comparing with Eq. (9) we observe $D \gg D_{min}$. In addition, we find a stairstep density profile, which is characteristic of the ideal multiple-mirror regime.[1] These similarities show that the viscous fluid regime and the ideal multiple-mirror regime have the same limiting properties in the transition region where neither is strictly valid.

Although ours has been a steady-state analysis, the existence of a diffusion coefficient allows for a straightforward extension to a time-dependent problem via the diffusion equation $\partial n/\partial t = \partial(D\partial n/\partial z)/\partial z$.

ACKNOWLEDGMENTS

This work was supported by Department of Energy Contract No. DE-AS03-76F00034, PA# DE-AT0E-76ET53059 and National Science Foundation Grant No. ENG-78-26372.

FOOTNOTES

[1]A. Makhijani, A. J. Lichtenberg, M. A. Lieberman, and B. Grant Logan, Phys. Fluids 17, 1291 (1974).

[2]V. V. Mirnov and D. D. Ryutov, Nucl. Fusion 12, 627 (1972).

[3]G. Miller, Los Alamos Scientific Laboratory Report No. LA-7580-MS, 1978.

[4]S. I. Braginskii, in Reviews of Plasma Physics, edited by M. A. Leontovich (Consultants Bureau, New York, 1965), Vol. 1, p. 205.

[5]J. M. Dawson and M. F. Uman, Nucl. Fusion 5, 242 (1965).

[6]A. H. Shapiro, The Dynamics and Thermodynamics of Compressible Fluid Flow (The Ronald Press, New York, 1953), Vol. 1.

[7]A. C. Hindmarsh, computer code GEAR (Lawrence Livermore Laboratory, Livermore, California, 1975).

TABLE I. Values of $f \equiv \frac{\ell_m}{\ell_c} \int_0^1 \frac{d\zeta}{a^3} \left(\frac{da}{d\zeta}\right)^2$ for typical values of R_m and ℓ_m/ℓ_c .

$\frac{\ell_m}{\ell_c}$	R_m				
	2	4	6	8	10
$\frac{1}{5}$	0.42	1.17	1.59	1.85	2.04
$\frac{1}{10}$	0.36	0.98	1.32	1.53	1.67
$\frac{1}{15}$	0.36	0.96	1.29	1.49	1.63
$\frac{1}{20}$	0.35	0.95	1.28	1.48	1.62

TABLE II. Values of $g \equiv \frac{1}{R_m}\int_0^1 d\zeta\, a$ for typical values of R_m and ℓ_m/ℓ_c.

$\frac{\ell_m}{\ell_c}$	R_m				
	2	4	6	8	10
$\frac{1}{5}$	0.80	0.64	0.56	0.50	0.47
$\frac{1}{10}$	0.88	0.77	0.71	0.67	0.64
$\frac{1}{15}$	0.92	0.84	0.79	0.76	0.74
$\frac{1}{20}$	0.94	0.88	0.84	0.82	0.79

LIST OF FIGURE CAPTIONS

FIG. 1. Multiple-mirror magnetic field profile.

FIG. 2. Normalized density $\eta \equiv n/n_o$ versus axial coordinate $\zeta \equiv z/\ell_c$ for subsonic flow (initial Mach number $M_o < 1$) and supersonic flow ($M_o > 1$). Here $\zeta_1 \equiv (\ell_m/\lambda_o)(1-M_o^2+M_o^2\ \ell n\ M_o^2)(2fM_o)^{-1}$.

FIG. 3. Normalized density $\eta \equiv n/n_o$ versus $\zeta \equiv z/\ell_c$ as determined numerically (solid lines) and analytically (dashed lines). All cases are with $R_m = 4$, $\ell_m/\ell_c = 0.1$, and $N = 18$. Ratio of initial mean-free-path λ_o to cell length ℓ_c is (a) 0.001 , (b) 0.01 , and (c) 0.05 .

FIG. 4. Ratio of confinement time τ_c to that of an $18\ell_c$ - long solenoid, $\tau_o \equiv 18\ell_c/2v_s$, versus λ_o/ℓ_c as determined numerically (triangles) and analytically (circles). Each set exhibits scaling with respect to (a) ℓ_m/ℓ_c , (b) R_m , and (c) N . The dashed curves in (a) represent constant values of λ_o/ℓ_m .

FIG. 5. Ratio of confinement time τ_c to that of a solenoid of length L , $\tau_o \equiv L/2v_s$, versus λ_o/ℓ_m in both the viscous fluid regime and ideal multiple-mirror regime. The dashed curve represents the form of the actual solution.

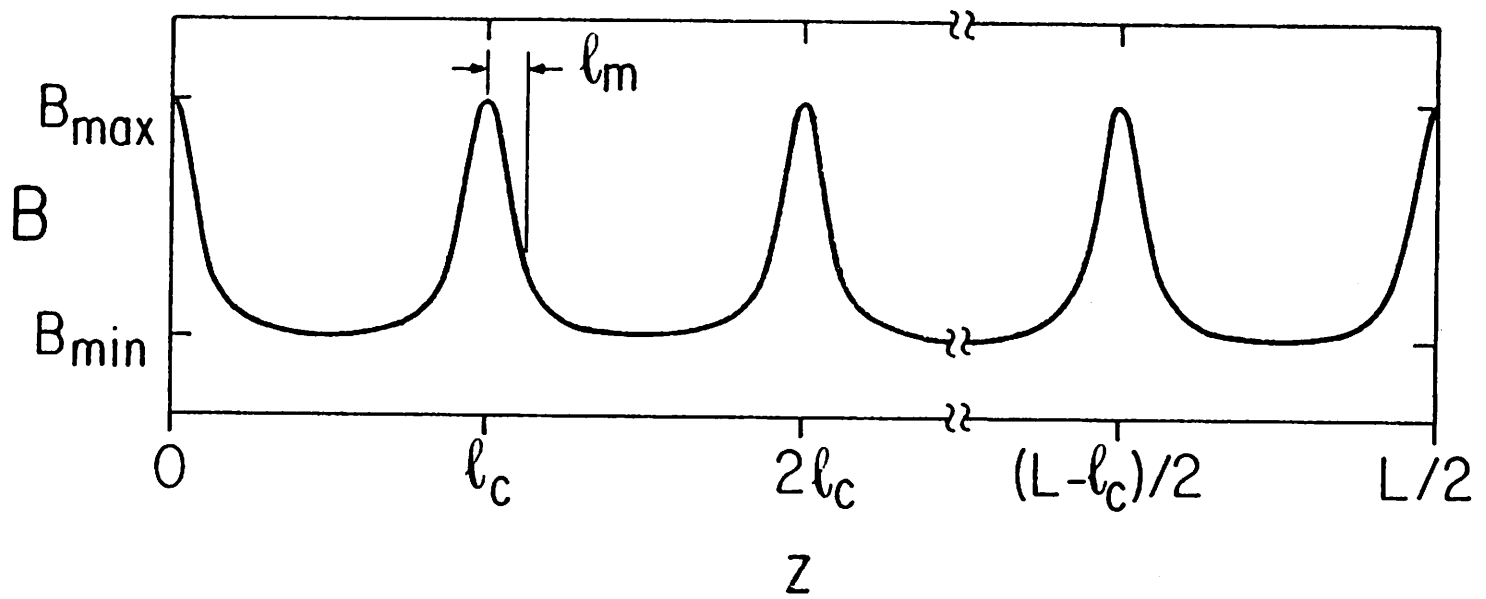

Figure 1.

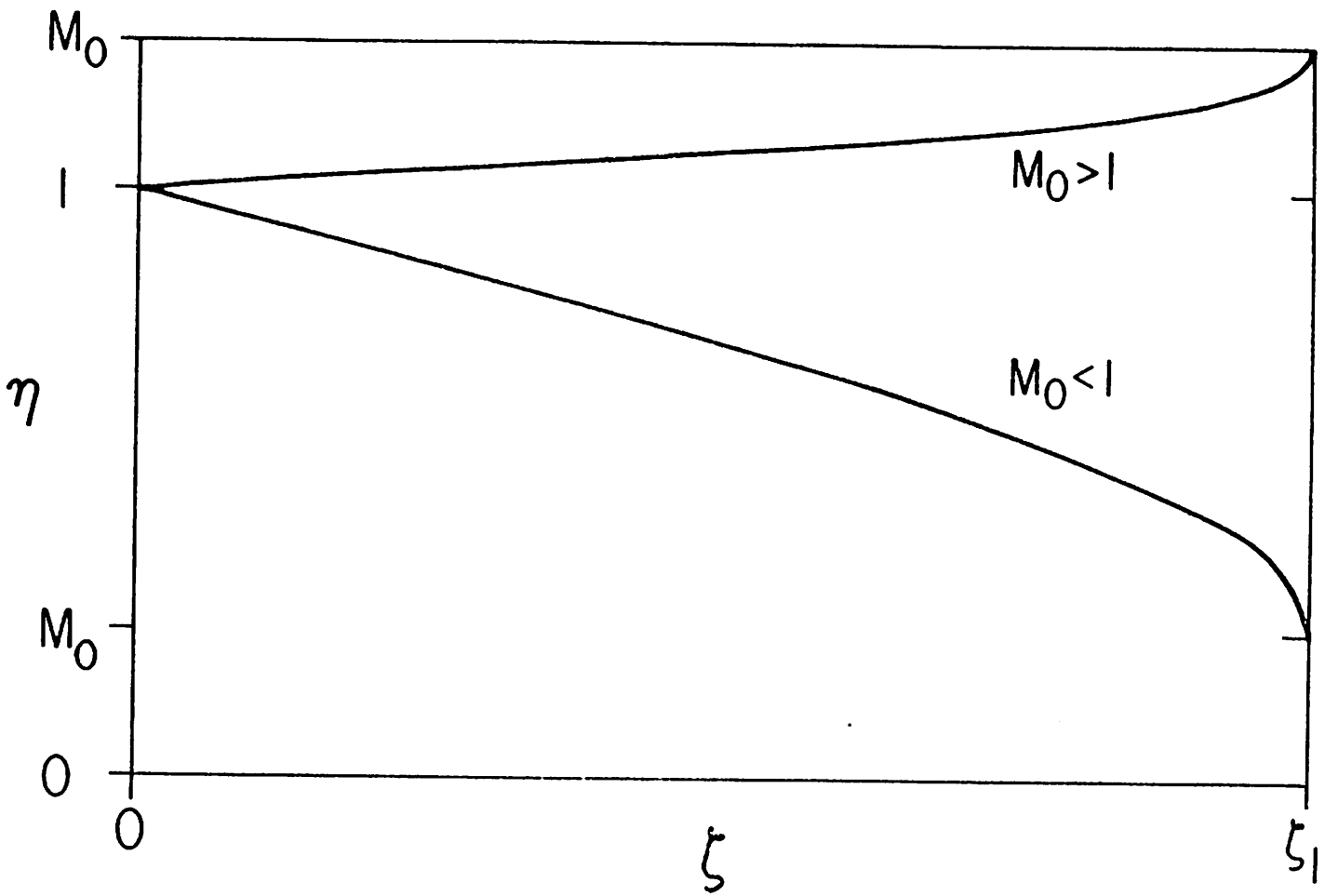

Figure 2.

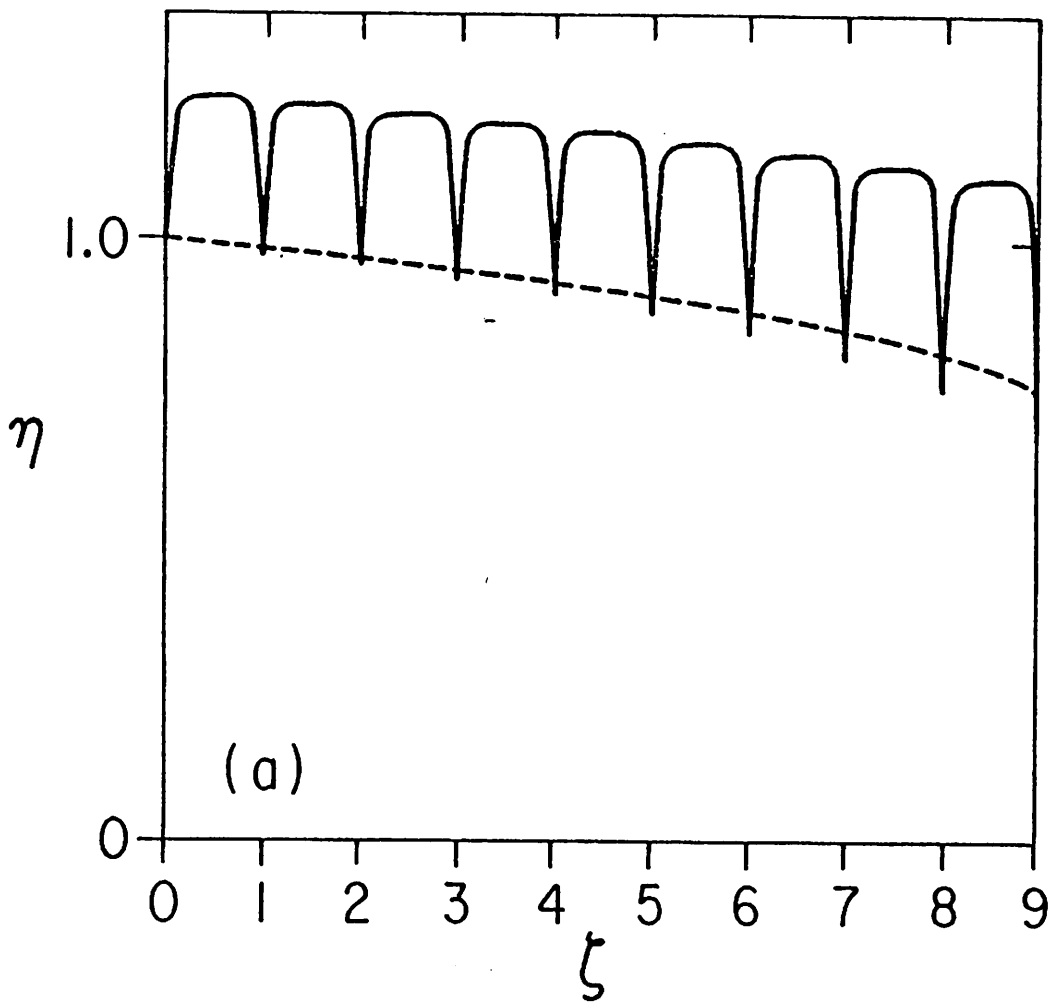

Figure 3(a).

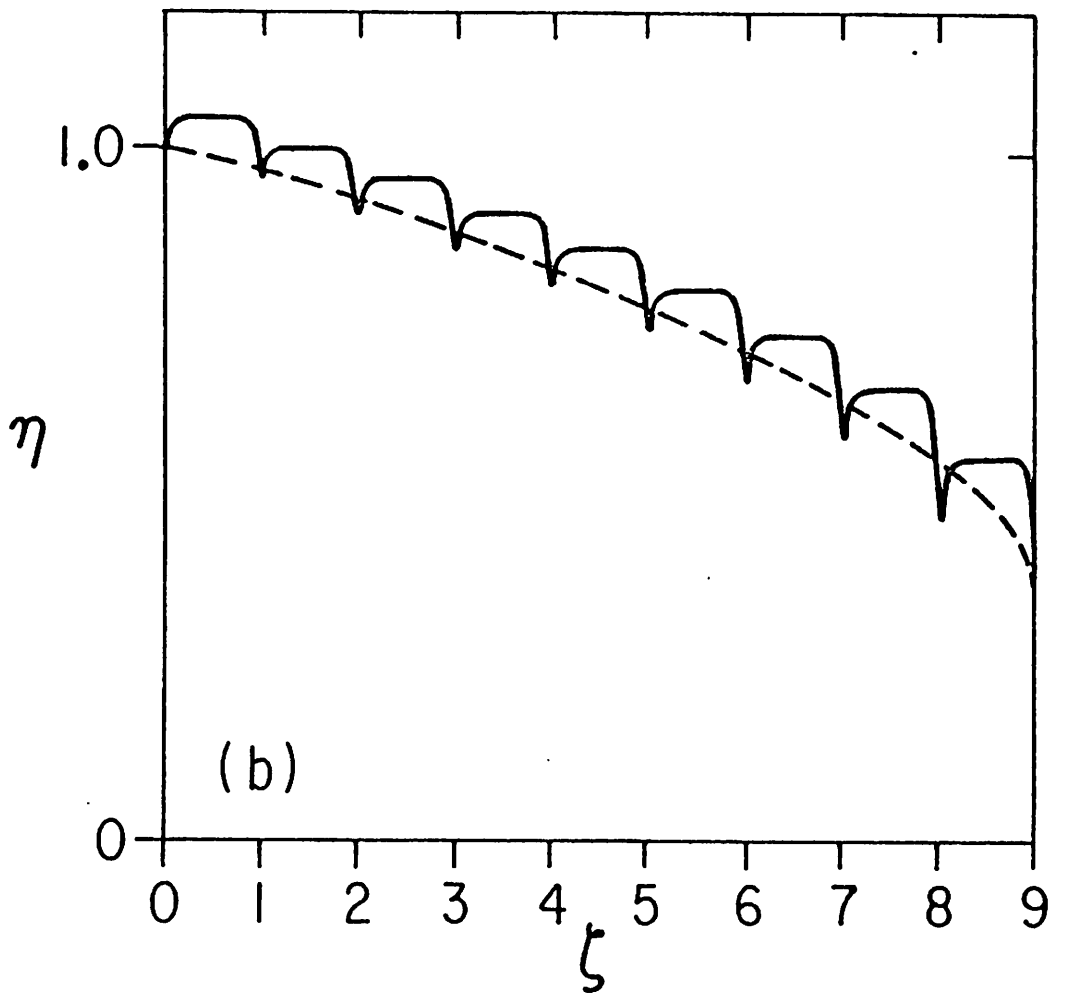

Figure 3(b).

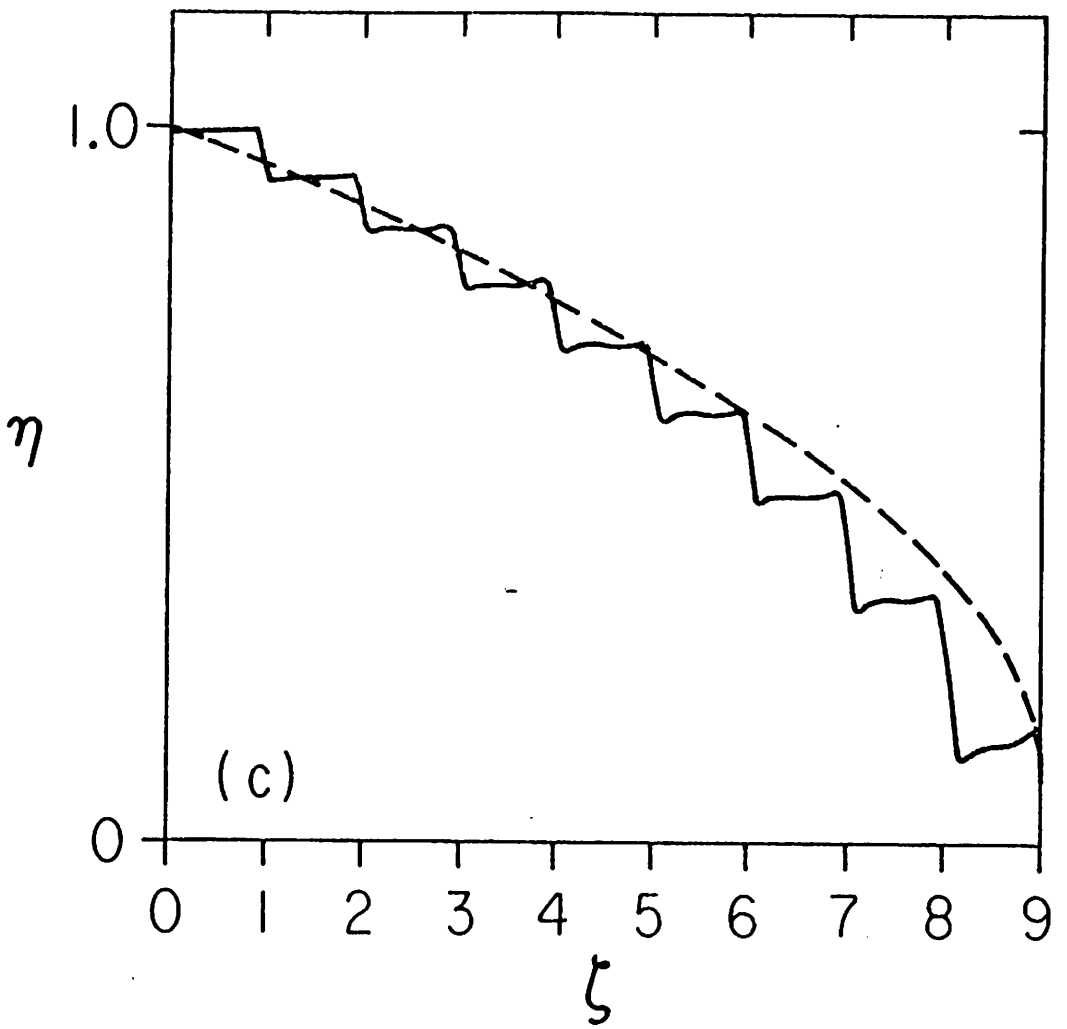

Figure 3(c).

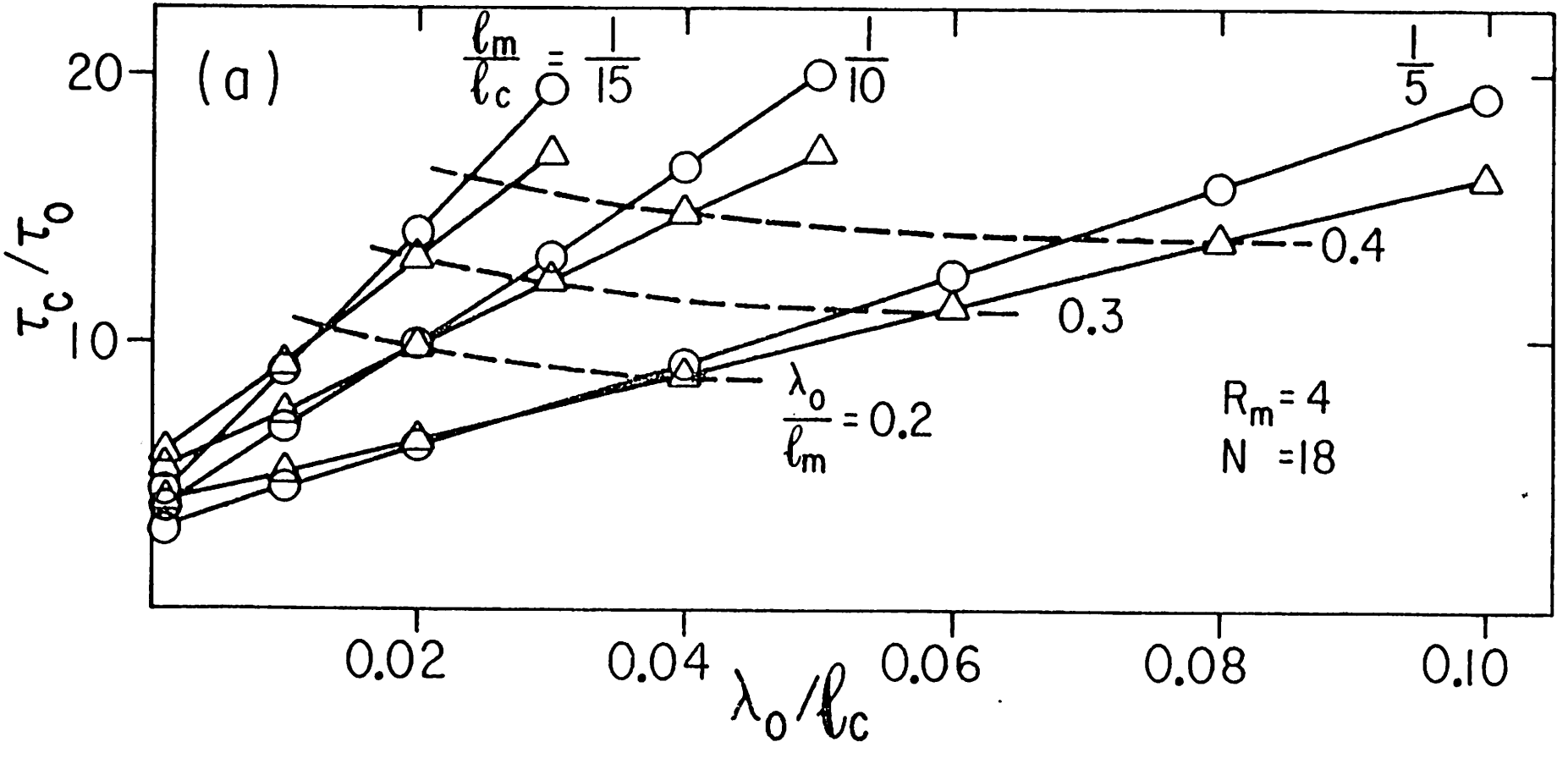
(a)
$\frac{\ell_m}{\ell_c} = \frac{1}{15}$
$\frac{1}{10}$
$\frac{1}{5}$
0.4
0.3
$\frac{\lambda_0}{\ell_m} = 0.2$
$R_m = 4$
N = 18
τ_c/τ_0
20
10
0.02
0.04
0.06
0.08
0.10
λ_0/ℓ_c

Figure 4(a).

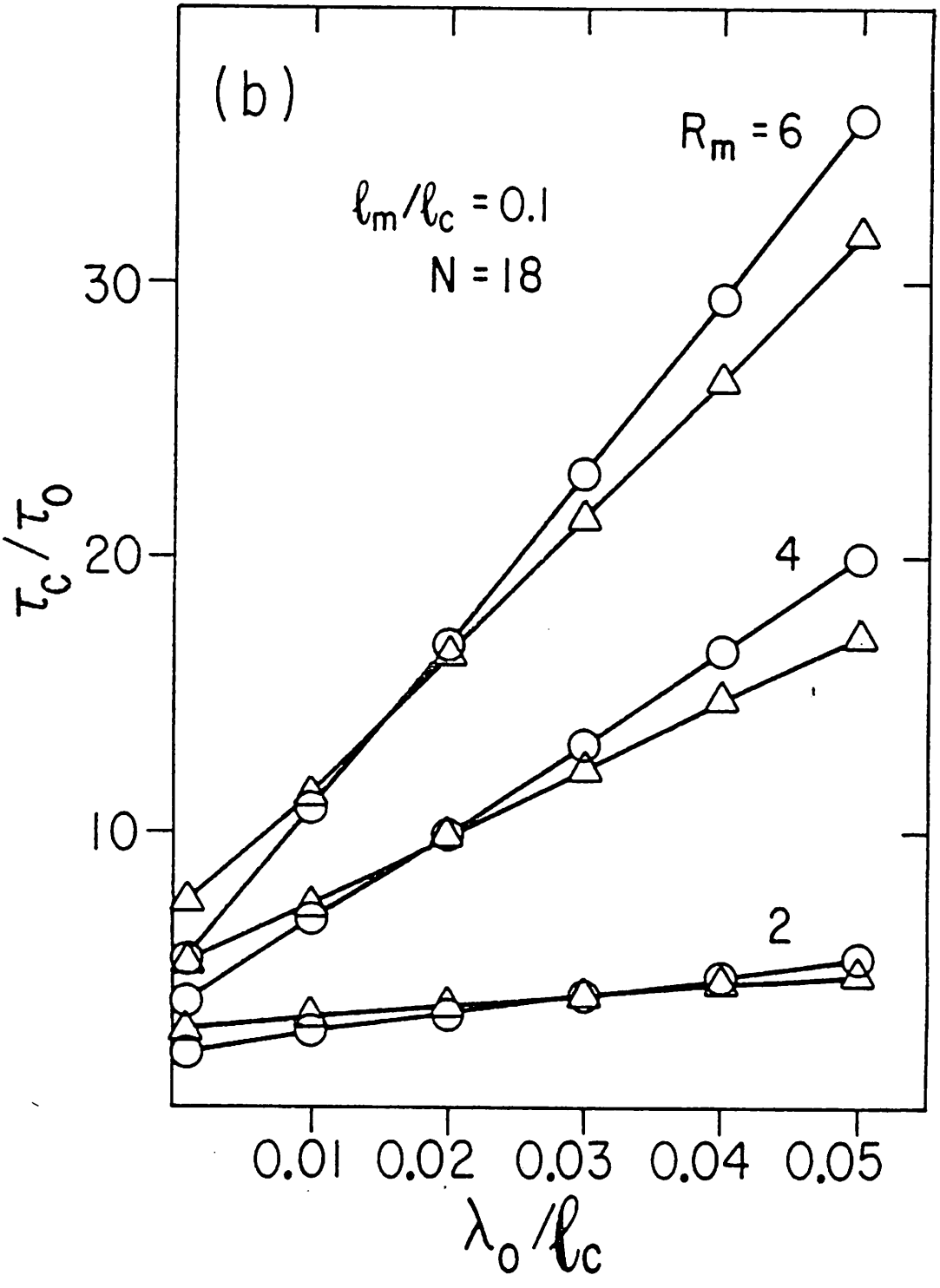
(b)
$R_m = 6$
$\ell_m/\ell_c = 0.1$
N = 18
4
2
30
20
10
τ_c/τ_0
0.01
0.02
0.03
0.04
0.05
λ_0/ℓ_c

Figure 4(b).

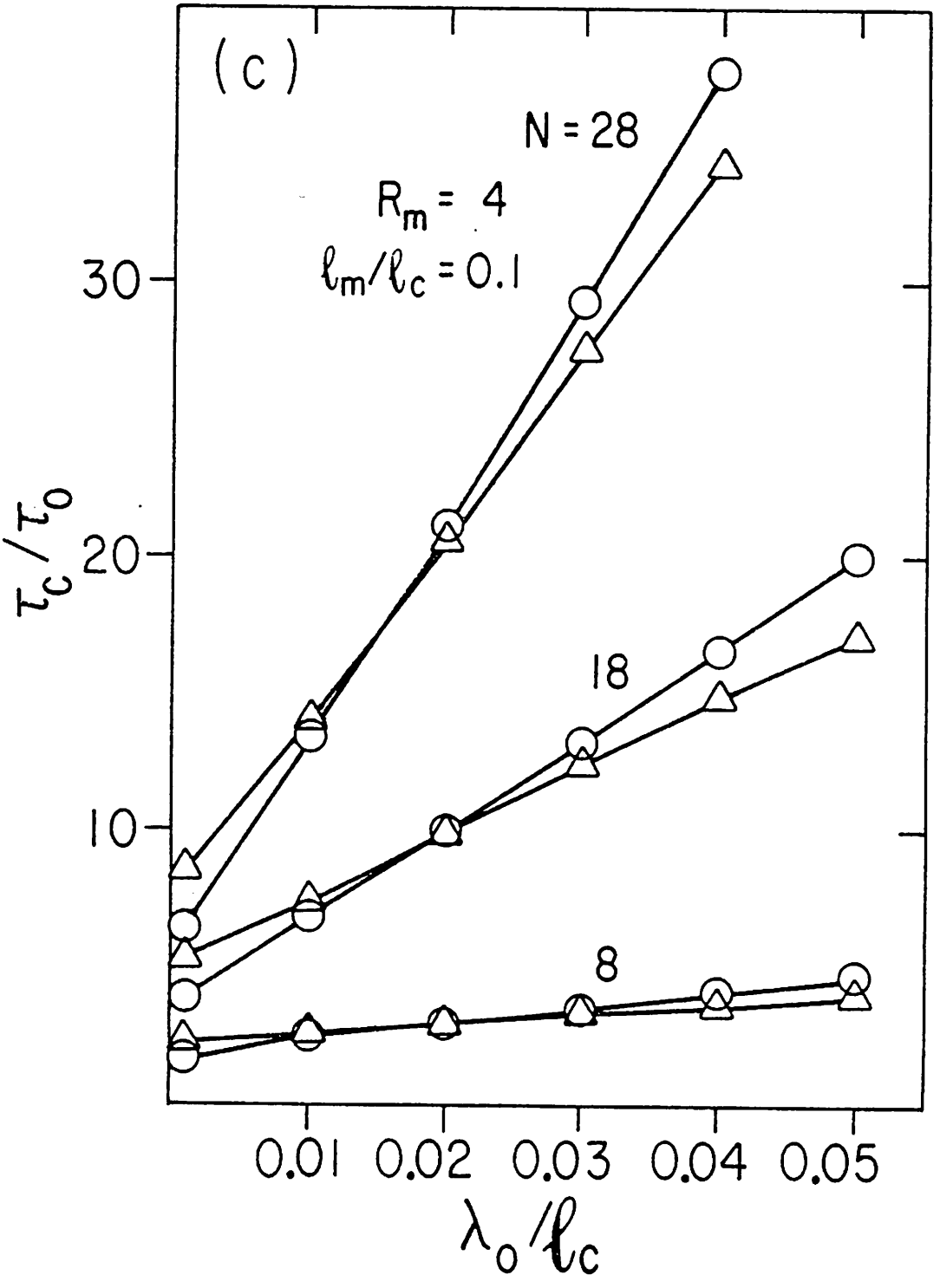
(c)
N = 28
R_m = 4
ℓ_m/ℓ_c = 0.1
30
20
10
τ_c/τ_0
18
8
0.01
0.02
0.03
0.04
0.05
λ_0/ℓ_c

Figure 4(c).

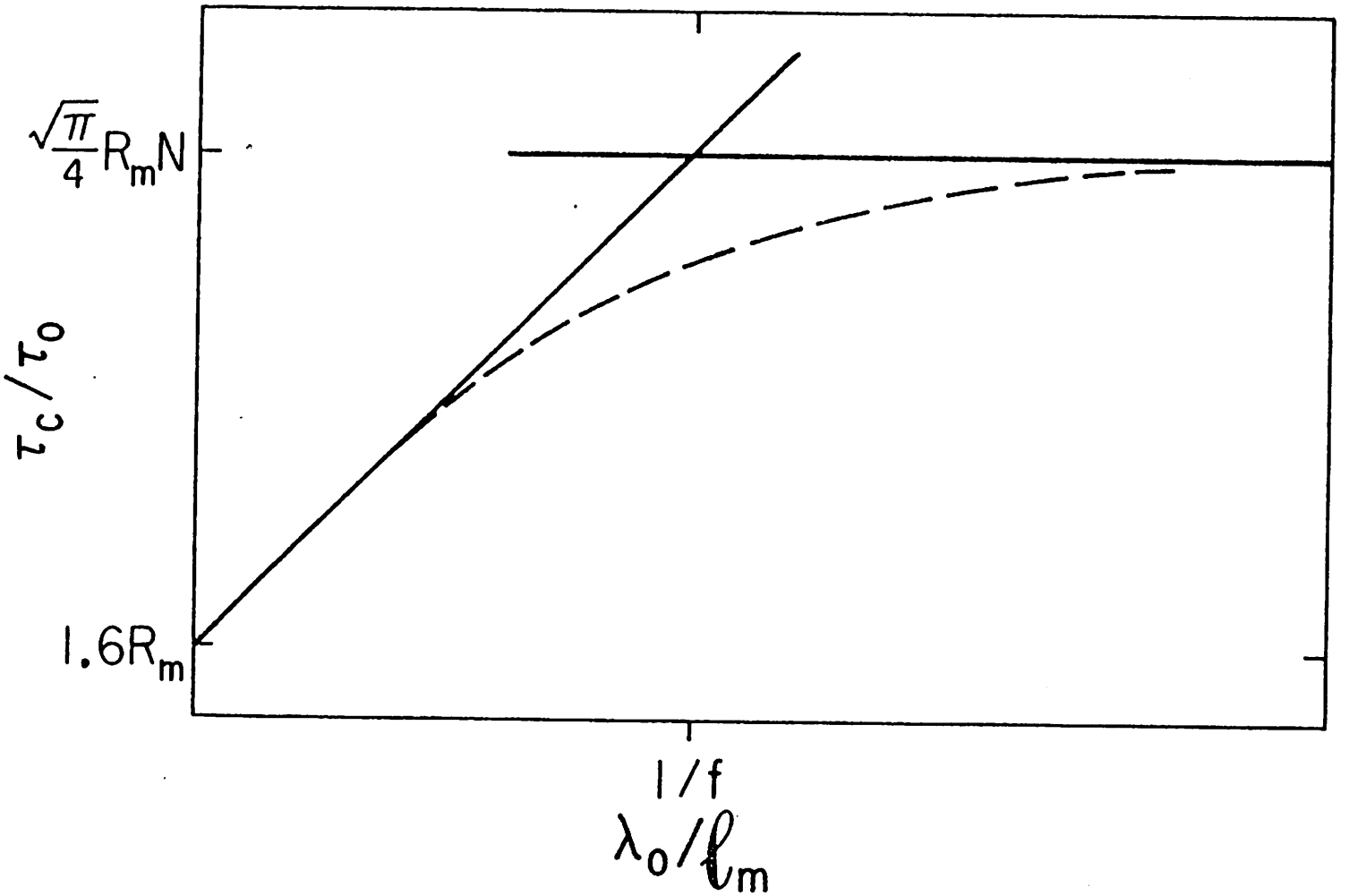

Figure 5.